NANO LETTERS

Letter

pubs.acs.org/NanoLett

Plasmonic Fano Nanoantennas for On-Chip Separation of Wavelength-Encoded Optical Signals

Rui Guo, Manuel Decker,* Frank Setzpfandt, Isabelle Staude, Dragomir N. Neshev, and Yuri S. Kivshar

Nonlinear Physics Centre and Centre for Ultrahigh Bandwidth Devices for Optical Systems (CUDOS), Research School of Physics and Engineering, The Australian National University, Canberra, ACT 2601, Australia

ABSTRACT: Here we suggest and realize an ultracompact plasmonic spectral-band demultiplexer for telecommunication wavelengths integrated onto an optical waveguide that couples two wavelength-encoded optical signals in the O- and the C-band in opposite directions of a silicon waveguide. In this way, we demonstrate a plasmonic key element for on-chip optical data processing that can also be used as a functional link between on- and off-chip optical signals.

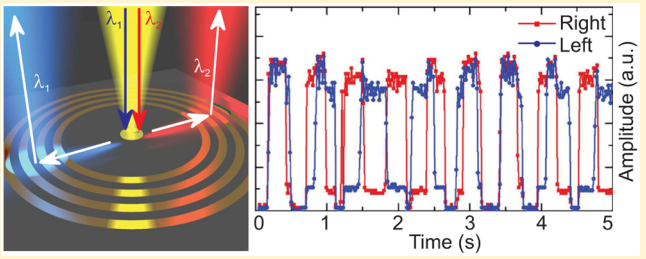

KEYWORDS: *Plasmonic nanoantenna, Fano resonance, on-chip integration, spectral-band demultiplexing*

Because of their ability to confine light to subwavelength volumes,[1] plasmonic nanoparticles and nanoantennas provide a fundamental link between electronic and photonic circuits as they can bridge the large size mismatch between the electronic and photonic wave functions.[2,3] As a result, plasmonic elements can be utilized to increase the integration density and performance of active and passive photonic devices. In this context, many ultrafast and compact devices with designed functionalities have been suggested, including plasmonic photodetectors,[4−8] modulators,[9,10] plasmonic waveguides,[2,11] and plasmonic waveguide couplers.[12−16] Furthermore, first experimental demonstrations of directional waveguide coupling have been reported very recently.[17−20] However, an ultracompact plasmonic realization of an optical demultiplexer that is suitable for on-chip signal processing is still missing. Here we suggest the concept of hybrid plasmonic-dielectric devices and realize an ultracompact plasmonic spectral-band demultiplexer for telecommunication wavelengths integrated onto an optical waveguide. In contrast to conventional large-scale optical wavelength demultiplexers based on prisms, gratings, Mach−Zehnder interferometers, or spectral filtering that are difficult to miniaturize, we develop and realize a submicron-sized nanoantenna supporting bidirectional waveguide coupling that additionally provides an interconnect between free-space and on-chip photonic circuitry. The key to the device functionality is to realize an antenna with the capability of simultaneously directing light of two different wavelengths in opposite directions. Since most of the conventional nanoantennas only provide unidirectional scattering characteristics,[21−25] these designs are not suitable for multiplexing applications. Bimetallic antenna designs[26] utilizing interband transitions of gold to realize bidirectional scattering are not suitable either since their operation frequency cannot be scaled to the technically relevant frequency range for silicon photonics. Our design utilizes the concept of Fano resonances[25,27−30] in plasmonic nanostructures for tailoring the nanoantenna scattering properties in order to separate two wavelength-encoded optical signals. We design our functional antenna to operate at near-infrared frequencies and integrate it onto a silicon waveguide to experimentally demonstrate on-chip spectral-band demultiplexing in the O- and the C-telecommunication bands. In this way, we demonstrate a plasmonic key element for on-chip optical data processing that can also be used as a functional link between on- and off-chip optical signals.

Unidirectional scattering or emission of radiation in commonly used nanoantenna designs like Yagi−Uda antennas,[21] for example, is typically achieved by detuning the resonance wavelengths of two or more antenna elements. In this way the relative phase differences in the radiation fields of the individual antenna elements are adjusted to realize constructive interference in one direction and destructive interference in the other direction. However, in order to be able to spatially separate optical signals encoded at different operation wavelengths one requires a nanoantenna that operates at (at least) two different wavelengths and supports unidirectional scattering in different directions at each operation wavelength. A solution to enable such multi-wavelength functionality is the use of Fano resonances,[27] which are known to provide an alternative way of designing far-field radiation patterns[25,30] and emission patterns of localized light sources.[28,29,31] However, the concept of Fano resonances has never been applied in order to design multidirectional scattering in plasmonic nanoantennas, the fundamental prerequisite for dividingwavelength-encoded optical signals.

Here, we effectively merge a rod-shaped aperture antenna (nanoslit) and a circular patch antenna (nanodisk) into one

Received: February 9, 2015
Revised: March 30, 2015
Published: April 6, 2015

DOI: 10.1021/acs.nanolett.5b00560
Nano Lett. 2015, 15, 3324−3328

compact subwavelength nanoparticle. These two elements combine a broad nanodisk resonance with a comparably narrow resonance from the nanoslit that are strongly coupled to each other via the electric currents within the single particle. As a result, they give rise to a Fano resonance in the scattering spectrum, which, in turn, enables directional scattering of light with different wavelengths in different directions. This Fano nanoantenna, which is designed for operation at the O- and the C-band in the near-infrared, is then processed on top of a silicon-slab waveguide on a silicon-on insulator (SOI) wafer that is used to guide the scattered light from the antenna. As a result our directional nanoantenna couples incident light of different wavelengths into different propagation directions in the slab-waveguide (see Figure 1a,b) and hence can be used to spatially separate optical signals. A scanning electron microscopy image of a typical Fano nanoantenna is depicted in Figure 1c. Furthermore, in order to detect the radiation that is coupled into different directions of the silicon waveguide by the nanoantenna, we process an additional gold ring-grating coupler centered on the nanoantenna (see Figure 1a,d). This allows us to measure the angle-resolved directivity pattern within the silicon waveguide and, most importantly, to separately detect the different wavelength-encoded optical signals at two opposite outputs.

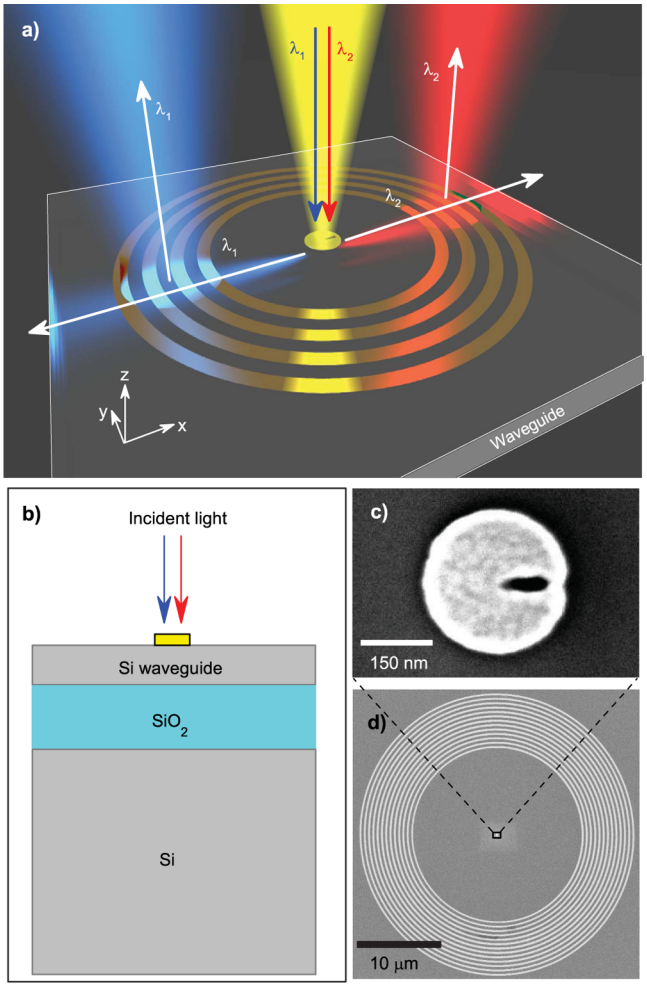

Figure 1. (a) Schematics of the wavelength-demultiplexing nanoantenna on a slab waveguide with a circular ring-grating for detection. (b) Experimental configuration of the nanoantenna on a silicon-on-insulator wafer. (c,d) Scanning electron microscope image of the fabricated nanoantenna (c) and the circular grating (d) on top of the silicon-slab waveguide.

In a first step, we numerically tailor the scattering properties of our bidirectional plasmonic Fano nanoantenna and identify the nanoantenna parameters for operation at the two telecommunication bands at λ_1 = 1310 nm (O-band) and λ_2 = 1550 nm (C-band). This results in a circular gold nanodisk with a diameter of d = 300 nm and a gold thickness of h = 30 nm and a 18 nm-wide and 100 nm-long nanoslit, which is displaced by 60 nm from the center of the disk in $+x$-direction. For the numerical calculations we use the finite-element frequency-domain solver of the software package CST Microwave Studio. In order clearly separate the Fano antenna properties from the influence of the waveguide substrate, we calculate the scattering properties of the nanodisk/nanoslit antenna alone, i.e., without substrate, but embedded in an effective medium that accounts for frequency shifts due to the influence of the SOI wafer in experiment. In this way, the functional mechanism of the antenna can be investigated and we can exclude that the waveguide substrate is responsible for the observed effect. The effective refractive index of the embedding medium (n = 2.1) was chosen so that the antenna resonances in the effective medium coincide with the resonances of the antenna on the waveguide substrate. We then excite the nanoantenna with a y-polarized plane wave incident from the top and calculate the normalized scattering cross section. Figure 2a shows the scattering cross section (black solid line) of the nanoantenna, which is characterized by a broad resonance with a pronounced maximum at $\lambda \approx$ 1900 nm wavelength and a resonance minimum at $\lambda \approx$ 1300 nm wavelength. To identify the origin of the resonances in our nanoantenna design, we separately analyze the constituent elements of the nanoantenna, namely, the gold nanodisk and the nanoslit. For the single gold nanodisk, i.e., without nanoslit, we find a broad resonance with a pronounced peak at approximately 1800 nm wavelength in the scattering cross section (red dashed line) that matches the main peak in the scattering cross section of the final nanoantenna design. In order to investigate the resonance properties of the nanoslit we calculate, inspired by Babinet's principle, the scattering properties of its complementary structure: a single gold nanorod identical in dimensions to the nanoslit (blue dashed line). The gold nanorod shows a pronounced and spectrally narrow resonance peak at approximately 1300 nm wavelength where the resonance dip for the final nanoantenna design is observed. This behavior is indeed evidence for the presence of a Fano resonance in the optical response of the combined nanodisk/nanoslit antenna since at this spectral position the narrow resonance of the nanoslit destructively interferes with the broad resonance of the nanodisk. In a second step, we numerically calculate the angle-resolved coupling directivity of the nanoantenna on top of a 220 nm-thin silicon slab waveguide, i.e., the intensity of light coupled in one waveguide direction normalized to the total intensity coupled into the waveguide, for the two operation wavelengths λ_1 (O-band) and λ_2 (C-band) of the antenna. These results are shown in Figure 2b and show that at $\lambda_1 \approx$ 1310 nm wavelength the nanoantenna has highly directional waveguide coupling with a maximum coupling directivity of around 7 to the left ($-x$-direction) of the waveguide, while at $\lambda_2 \approx$ 1550 nm wavelength the light is coupled to the right with a directivity of around 6. Hence, our

DOI: 10.1021/acs.nanolett.5b00560
Nano Lett. 2015, 15, 3324−3328

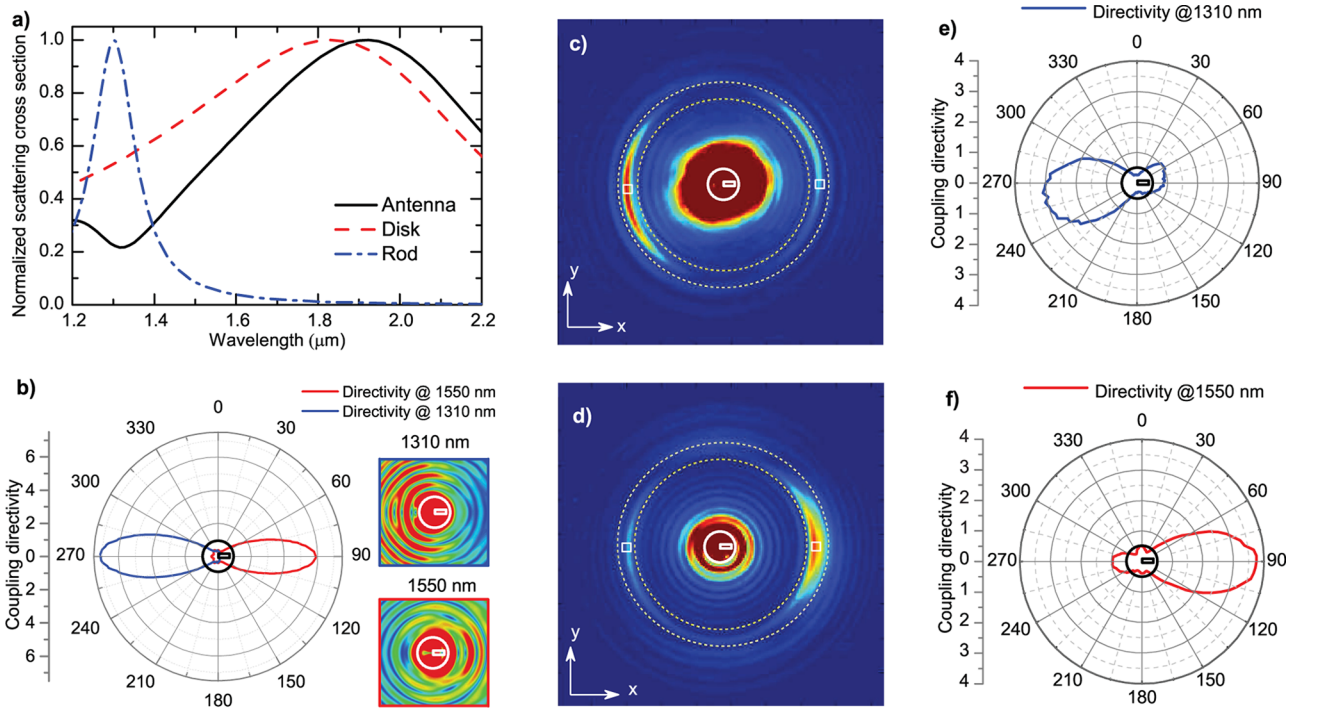

Figure 2. (a) Calculated scattering cross section of the nanoantenna embedded in a medium with n = 2.1 and its constituent elements, a gold nanodisk and a nanorod. (b) Calculated directivity of light coupling into the waveguide for the two operation wavelengths. (c,d) Experimental CCD image (raw data) for y-polarized illumination of the antenna at a wavelength of (c) λ_1 = 1310 nm and (d) λ_2 = 1550 nm. The antenna (not to scale) is indicated as a white outline. (e,f) Directivity extracted from (c,d) by evaluation of the out-coupled power from the ring grating [white-dashed lines in (c,d)].

nanoantenna supports two-directional waveguide coupling when integrated onto a silicon waveguide.

Next, we fabricate the nanoantenna on a silicon-on insulator wafer (see Figure 1b). To detect the radiation that is coupled into different directions of the silicon waveguide by the nanoantenna we image the light that is coupled out by a circular grating onto an InGaAs CCD camera (Figure 2c,d). In this way, we can spatially separate and analyze two wavelength-encoded optical signals. Furthermore, the circular ring grating allows us to directly extract the angle-resolved directional coupling pattern into the silicon waveguide for the two operation wavelengths λ_1 and λ_2 separately. These measured patterns are shown in Figure 2e,f and confirm directional waveguide coupling of the incident light to the left and right with a maximum coupling directivity of approximately 3 and 4, respectively. The slight angular rotation of the directional-coupling pattern for λ_1 = 1310 nm wavelength can be attributed to fabrication imperfections of the nanoantenna. In order to estimate the coupling efficiencies of light into the waveguide at the two operation wavelengths, we calculate the ratio of the power collected from the left/right half of the ring grating divided by the power of the incident light and obtain coupling efficiencies of 3.3% for λ_1 = 1310 nm wavelength and 5.8% for λ_2 = 1550 nm wavelength, respectively. These waveguide-coupling efficiencies assume a grating out-coupling efficiency of about 25% for λ_1 = 1310 nm and 30% for λ_2 = 1550 nm gained from numerical simulations.

Finally, we demonstrate on-chip spectral band separation with the use of our Fano nanoantenna on the silicon waveguide. We modulate the light of two laser sources at two different modulation frequencies ($f_1 = f_{\lambda 1}$ = 1.48 Hz; $f_2 = f_{\lambda 2}$ = 1.78 Hz) utilizing a two-frequency chopper and combine the two signals into a single beam with a beam splitter. We then focus the combined laser beam onto the sample (see Figure 3a). The two wavelength-encoded signals are then directionally coupled into the waveguide by the nanoantenna. After propagation to the left/right, the light is out-coupled by the circular grating on the left/right. We then monitor the time-dependent total intensity $I_{tot} = I_{\lambda 1} + I_{\lambda 2}$ at each of the two opposite output ports (white rectangles in Figure 2c,d) by evaluation of the CCD camera images at the positions shown in Figure 2c. The measured signal at the output port on the left and on the right is plotted in Figure 3b in blue and red, respectively, depicting the time-traces of a typical signal recorded at the respective ports in a time interval of five seconds. For each port on the waveguide the corresponding wavelength-encoded signals with the two frequencies f_1 = 1.48 Hz and f_2 = 1.78 Hz are nicely separated and recovered. In order to clearly identify the frequency-components that are measured, we perform a Fourier analysis of a 2.5 min-long time-trace at each output port. From the frequency analysis shown in Figure 3c we can identify two frequency peaks, one main peak at each port, at the two modulation frequencies of the combined input beam confirming that the two modulated signals are very well separated by this wavelength-demultiplexing nanoantenna. The width of each resonance and hence the frequency spread of the two signals are mainly determined by the frequency variation of the input signal due to the chopper used in the experiment. Notably, the operation frequency of our wavelength demultiplexing integrated nanoantenna is only limited by the technical limitations of the camera used in the experiment, which is fixed to a sampling rate of 59 frames per seconds. There is no fundamental limit for operation at THz modulation frequencies. In principle, our design can also be used to enable

DOI: 10.1021/acs.nanolett.5b00560
Nano Lett. 2015, 15, 3324−3328

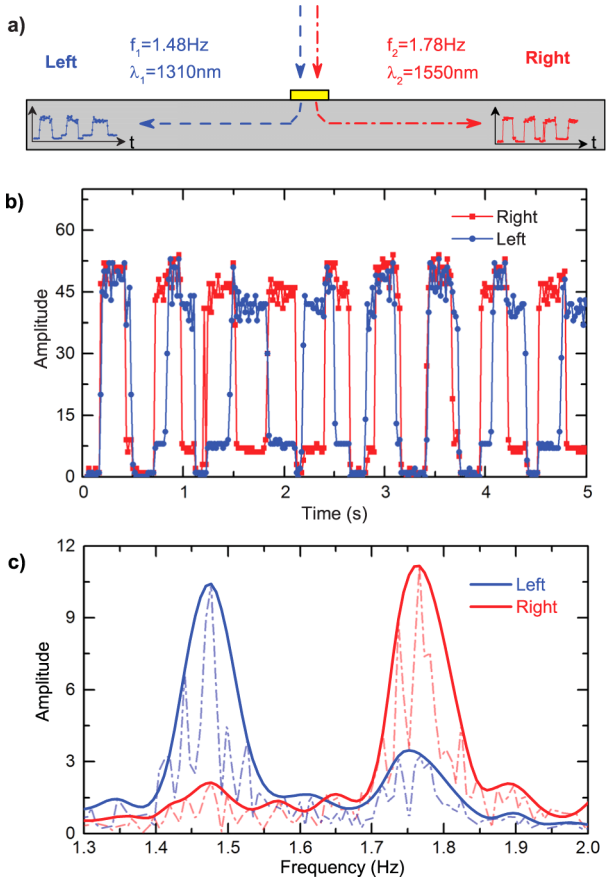

Figure 3. (a) Schematics of the experiment. Two optical signals with f_1 = 1.48 Hz, f_2 = 1.78 Hz are encoded at λ_1 = 1310 nm, λ_2 = 1550 nm wavelength and coupled to the left, right by the nanoantenna. The corresponding signals are out-coupled by the grating and detected by a CCD camera. (b) Detected time signal at the left and the right output port and (c) Fourier analysis of the detected intensity at the two outputs confirming that the two original signals have been well separated by the nanoantenna. The raw data are plotted as dash-dotted lines with the corresponding envelopes (solid lines).

multichannel wavelength demultiplexing if the frequency spacing of the resonances is decreased, and the number of channels is increased. Since the quality factor of the (narrow) nanoslit resonance ultimately determines the frequency spacing, a reduction of the frequency spacing can be achieved by increasing the quality factor of the narrow resonance, e.g., by using dark modes in more complex plasmonic particles or by using low-loss dielectric nanoparticles that have been investigated recently.[32,33] Also, the general strategy of hybridizing low-loss dielectric waveguide architectures with plasmonic nanoparticles can be extended to support a larger number of channels by using compact plasmonic structures with higher information density as, for example, provided by more complex antenna designs or multielement disordered photonic systems.

In conclusion, we have demonstrated an ultracompact plasmonic spectral-band demultiplexer for telecommunication wavelengths integrated onto an optical waveguide that couples two wavelength-encoded optical signals in the O- and the C-bands in opposite directions of a silicon waveguide. We make use of the concept of Fano resonances in order to realize a single-particle plasmonic nanoantenna that supports bidirectional scattering and can, therefore, be used as the functional element for spectral-band demultiplexing. Furthermore, this nanoantenna can be deployed as either a functional element connecting two optical waveguides or as a functional link between off-chip signals and on-chip optical circuitry. Hence, this spectral band division plasmonic nanoantenna provides an ultracompact functional element for on-chip optical circuitry.

AUTHOR INFORMATION

Corresponding Author

*E-mail: manuel.decker@anu.edu.au.

Notes

The authors declare no competing financial interest.

ACKNOWLEDGMENTS

The authors thank G. Li, M. Liu, N. Shahid, and K. Vora for useful discussions and acknowledge support from the Australian Research Council through Discovery Project and DECRA Fellowship grants.

REFERENCES

(1) Schuller, J. A.; Barnard, E. S.; Cai, W.; Jun, Y. C.; White, J. S.; Brongersma, M. L. *Nat. Mater.* **2010**, *9*, 193−204.
(2) Gramotnev, D. K.; Bozhevolnyi, S. I. *Nat. Photonics* **2010**, *4*, 83−91.
(3) Zia, R.; Schuller, J. A.; Chandran, A.; Brongersma, M. L. *Mater. Today* **2006**, *9*, 20−27.
(4) Konstantatos, G.; Sargent, E. H. *Nat. Nanotechnol.* **2010**, *5*, 391−400.
(5) Knight, M. W.; Sobhani, H.; Nordlander, P.; Halas, N. J. *Science* **2011**, *332*, 702−704.
(6) Goykhman, I.; Desiatov, B.; Khurgin, J.; Shappir, J.; Levy, U. *Nano Lett.* **2011**, *11*, 2219−2224.
(7) Sobhani, A.; Knight, M. W.; Wang, Y.; Zheng, B.; King, N. S.; Brown, L. V.; Fang, Z.; Nordlander, P.; Halas, N. J. *Nat. Commun.* **2013**, *4*, 1643.
(8) Chalabi, H.; Schoen, D.; Brongersma, M. L. *Nano Lett.* **2014**, *14*, 1374−1380.
(9) Cai, W.; White, J. S.; Brongersma, M. L. *Nano Lett.* **2009**, *9*, 4403−4411.
(10) Melikyan, A.; et al. *Nat. Photonics* **2013**, *8*, 229−233.
(11) Bozhevolnyi, S. I.; Volkov, V. S.; Devaux, E.; Laluet, J.- Y.; Ebbesen, T. W. *Nature* **2006**, *440*, 508−511.
(12) Lopez-Tejeira, F.; Rodrigo, S. G.; Martin-Moreno, L.; Garcia-Vidal, F. J.; Devaux, E.; Ebbesen, T. W.; Krenn, J. R.; Radko, I. P.; Bozhevolnyi, S. I.; Gonzalez, M. U.; Weeber, J. C.; Dereux, A. *Nat. Phys.* **2007**, *3*, 324−328.
(13) Liu, J. S. Q.; Pala, R. A.; Afshinmanesh, F.; Cai, W.; Brongersma, M. L. *Nat. Commun.* **2011**, *2*, 525.
(14) Baron, A.; Devaux, E.; Rodier, J.-C.; Hugonin, J.-P.; Rousseau, E.; Genet, C.; Ebbesen, T. W.; Lalanne, P. *Nano Lett.* **2011**, *11*, 4207−4212.
(15) Liu, Y.; Palomba, S.; Park, Y.; Zentgraf, T.; Yin, X.; Zhang, X. *Nano Lett.* **2012**, *12*, 4853−4858.
(16) Lin, J.; Mueller, J. P. B.; Wang, Q.; Yuan, G.; Antoniou, N.; Yuan, X.-C.; Capasso, F. *Science* **2013**, *340*, 331−334.
(17) Rodriguez-Fortuno, F. J.; Marino, G.; Ginzburg, P.; O'Connor, D.; Martinez, A.; Wurtz, G. A.; Zayats, A. V. *Science* **2013**, *340*, 328−330.
(18) Petersen, J.; Volz, J.; Rauschenbeutel, A. *Science* **2014**, *346*, 67−71.
(19) Sidiropoulos, T. P. H.; Nielsen, M. P.; Roschuk, T. R.; Zayats, A. V.; Maier, S. A.; Oulton, R. F. *ACS Photonics* **2014**, *1*, 912−916.
(20) Piggott, A. Y.; Lu, J.; Babinec, T. M.; Lagoudakis, K. G.; Petykiewicz, J.; Vuckovic, J. *Sci. Rep.* **2014**, *4*, 7210.
(21) Novotny, L.; van Hulst, N. F. *Nat. Photonics* **2011**, *5*, 83−90.
(22) Staude, I.; Maksymov, I. S.; Decker, M.; Miroshnichenko, A. E.; Neshev, D. N.; Jagadish, C.; Kivshar, Y. S. *Phys. Status Solidi RRL* **2012**, *6*, 466−468.

DOI: 10.1021/acs.nanolett.5b00560
Nano Lett. 2015, 15, 3324−3328

(23) Liu, W.; Miroshnichenko, A. E.; Neshev, D. N.; Kivshar, Y. S. *ACS Nano* **2012**, *6*, 5489−5497.
(24) Dregely, D.; Taubert, R.; Dorfmüller, J.; Vogelgesang, R.; Kern, K.; Giessen, H. *Nat. Commun.* **2011**, *2*, 267.
(25) Vercruysse, D.; Sonnefraud, Y.; Verellen, N.; Fuchs, F. B.; Di Martino, G.; Lagae, L.; Moshchalkov, V. V.; Maier, S. A.; Van Dorpe, P. *Nano Lett.* **2013**, *13*, 3843−3849.
(26) Shegai, T.; Chen, S.; Miljkovic, V. D.; Zengin, G.; Johansson, P.; Käll, M. *Nat. Commun.* **2011**, *2*, 481.
(27) Luk'yanchuk, B.; Zheludev, N. I.; Maier, S. A.; Halas, N. J.; Nordlander, P.; Giessen, H.; Chong, C. T. *Nat. Mater.* **2010**, *9*, 707−715.
(28) Rybin, M. V.; Kapitanova, P. V.; Filonov, D. S.; Slobozhanyuk, A. P.; Belov, P. A.; Kivshar, Y. S.; Limonov, M. F. *Phys. Rev. B* **2013**, *88*, 205106.
(29) Artar, A.; Yanik, A. A.; Altug, H. *Nano Lett.* **2011**, *11*, 3694−3700.
(30) Guo, R.; Decker, M.; Staude, I.; Neshev, D. N.; Kivshar, Y. S. *Appl. Phys. Lett.* **2014**, *105*, 053114.
(31) Alavi Lavasani, S. H.; Pakizeh, T. *J. Opt. Soc. Am. B* **2012**, *29*, 1361−1366.
(32) Rusak, E.; Staude, I.; Decker, M.; Sautter, J.; Miroshnichenko, A. E.; Powell, D. A.; Neshev, D. N.; Kivshar, Y. S. *Appl. Phys. Lett.* **2014**, *105*, 221109.
(33) Decker, M.; Staude, I.; Falkner, M.; Dominguez, J.; Neshev, D. N.; Brener, I.; Pertsch, T.; Kivshar, Y. S. *Adv. Opt. Mater.* **2015**, DOI: 10.1002/adom.201400584.

DOI: 10.1021/acs.nanolett.5b00560
Nano Lett. 2015, 15, 3324−3328